Negative Curvature Hollow-Core Optical Fiber

Fei Yu and Jonathan C. Knight

(Invited Paper)

***Abstract*—The background, optical properties, and applications of low-loss negative curvature hollow-core fiber are reviewed. Data on spectral attenuation are collated and extended.**

***Index Terms*—Fiber optics, microstructured optical fiber.**

I. Introduction

NEGATIVE curvature hollow core optical fiber (NC-HCF) is a novel hollow core optical fiber (HCF) which has emerged over the last few years (Fig. 1) [1]–[8]. NC-HCF is characterized by the inverted curvature of its core wall, and usually exhibits multiple spectral transmission bands of low attenuation. The simple structure of the fiber cladding allows flexible tailoring of NC-HCFs design and dimension for specific wavelengths and applications [4], [5], [7], [9]. Since their first appearance NC-HCFs have been applied in high power/ultrafast laser delivery [10]–[14] and several other applications [15]–[20].

This paper comprises eight sections: Section II consists of a brief history of NC-HCF, while the optics of NC-HCF will be discussed in Section III. From Sections IV to VI the guidance properties of NC-HCFs are collated and summarized including mode attenuation, bending loss, dispersion and nonlinearity. Section VII reviews some applications of NC-HCFs and Section VIII contains conclusions.

II. A Brief History

A long time ago, "hollow core optical waveguides" referred to long cylindrical tubes and rectangular stripes made of dielectric or even metal.

In 1936, Carson *et al.* studied the potential of hollow core fiber made of metal material for long haul electromagnetic wave transmission theoretically [21]. Later, in 1964, Marcatili and Schmeltzer studied the feasibility of using the dielectric HCF in telecommunications [22]. They demonstrated analytically that the trade-off between modal leaky loss and bending loss would fundamentally limit the application of dielectric hollow core fiber for long-haul optical signal transmission. Nevertheless, through advances in inner-surface coating techniques, HCF achieved great successes in some fields such as mid-infrared light transmission, particularly in CO_2 laser delivery for industrial applications [23].

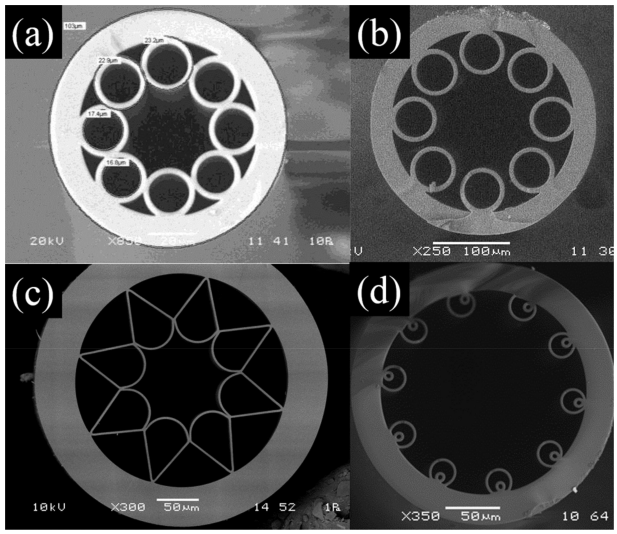

Fig. 1. SEM pictures of typical NC-HCFs (a) NC-HCF made of silica, with capillaries in touch in the cladding [1] (b) NC-HCF made of silica, with non-touching capillaries in the cladding [5] (c) NC-HCF made of silica with ice-cream-cone shape capillary in the cladding [3] (d) NC-HCF made of silica, with non-touching capillaries. Extra capillaries are added to reduce the coupling between the core and cladding modes [33].

By the end of the 20th century, the emergence of hollow core photonic bandgap fiber (HC-PBG) speeded up the development of HCFs in both theory and applications enormously [24], [25]. On one hand, it brought in new concepts of light guidance in HCFs and boosted the development of fiber optics; and on the other hand, it creatively introduced micro-structure into optical fiber design, and inspired more novel designs of optical fibers. The state-of-the-art HC-PBGs already demonstrate extremely low transmission loss, comparable to that of commercial optical fibers [26], [27].

"Kagome" fiber was another important type of HCFs that was firstly reported in 2002 [28]. The Kagome fiber usually exhibits multiple transmission bands and overall covers a broader spectral range than HC-PBGs. Numerical simulations show that the "Kagome" lattice supports no photonic bandgap which make the Kagome fiber distinctive [25], [29].

The appearance of NC-HCF can be traced back to the discovery of the importance of core wall shape in Kagome fiber in 2010 [30]. A Kagome fiber with negative curvature core boundary unexpectedly exhibited a lower attenuation than regular ones. A series of subsequent experiments confirmed the significance of core wall shape in the reduction of attenuation in such fibers [31].

Manuscript received June 14, 2015; revised August 17, 2015; accepted August 17, 2015. Date of publication August 26, 2015; date of current version October 13, 2015. This work was supported in part by the U.K. Engineering and Physical Sciences Research Council under Grant EP/I011315/1. This paper is self-contained in terms of unpublished data.

The authors are with the Department of Physics, Centre for Photonics and Photonic Materials, University of Bath, Bath BA2 7AY, U.K. (e-mail: fy230@bath.ac.uk; J.C.Knight@bath.ac.uk).

Color versions of one or more of the figures in this paper are available online at http://ieeexplore.ieee.org.

Digital Object Identifier 10.1109/JSTQE.2015.2473140

In 2011, Pryamikov and his colleagues fabricated the first NC-HCF for 3 μm wavelength transmission [1]. A 63 cm long NC-NCF was fabricated and several transmission bands were observed from 1 to 4 μm. Afterwards, Kosolapov *et al.* extended the transmission window to 10.6 μm for CO_2 laser delivery by using chalcogenide glass [2].

In 2012, a silica NC-HCF with low loss transmission in the mid-infrared spectral region from 3 to 4 μm was fabricated with minimum attenuation of 34 dB/km [3]. This type of NC HCF is characterized by "ice-cream-cone" shaped cladding capillaries, which are formed during the fiber drawing by the balance between gas pressure in the holes pressure and the surface tension of fiber material. Such fiber was later successfully demonstrated to deliver high energy microsecond pulses at 2.94 μm for invasive surgical laser procedure proposal [10], [11]. Attenuation figures of 24.4 and 85 dB/km were subsequently recorded in NC-HCFs of similar structure at 2.4 and 4 μm wavelength, respectively [9].

After demonstration in the mid-infrared spectral region, low loss NC-HCFs for shorter wavelength transmission in the visible and near-infrared were developed [13], [14], [18]. Recently, NC-HCF with attenuation of 0.15 and 0.18 dB/m at 532 and 515 nm, respectively achieved single-mode, stable transmission of nanosecond and picosecond pulses with 0.57 mJ and 30 μJ [13]. 40 dB/km was measured at 1064 nm in NC-HCF which was used as part of ring cavity in a mode-locked Ytterbium fiber laser with 37–11 MHz repetition rate [18].

Early in 2013, Kolyadin *et al.* reported the first design of open boundary of core wall in NC-HCF. This type of NC-HCF has contactless capillary cladding, and demonstrated low loss transmission of light in the mid-infrared spectrum range from 2.5 to 7.9 μm [5]. In 2014, greatly reduced bending loss in similar fibers was reported by Belardi *et al*. [8], [32]. This design was soon applied to shorter wavelength transmission in the near-infrared spectrum [33].

In 2013, THz guidance in NC-HCF made of polymethylmethacrylate was demonstrated by Setti *et al.* [4].

A further design variation of NC-HCF was proposed by Belardi and Knight in 2014 [6]. By adding extra anti-resonant elements in the cladding, numerical simulations predicted that the minimum loss of NC-HCFs could reach below 1 dB/km [6], [33].

Besides high power laser delivery [10]–[14], NC-HCFs have been also applied in the study of gas-light interaction. Stimulated Raman scattering in H_2 and C_2H_2 gas lasing were realized in NC-HCFs [15]–[17], [19], [20]. Further information can be found in Section VII.

III. Modeling and Analysis

NC-HCF has a simple structure compared to that of HC-PBG and Kagome fiber [25], [29]. It has no periodic cladding, and does not possess a photonic bandgap, which explains the leaky nature of such fiber. The leaky nature and antiresonant guiding mechanism make it natural to compare NC-HCF with Kagome fiber. Both have multiple transmission bands and similar attenuation figures at comparable wavelengths [34], [35]. Indeed, seeing the cladding of a Kagome fiber can be reduced to just one single layer without significantly increasing attenuation [36] we suspect that the guidance in these two fiber designs is very similar.

However, the simple geometry of NC-HCF belies the lack of a simple quantitative model of its optical performance. Currently the modeling of NC-HCFs depends heavily on numerical simulations. The Marcatili and Schmeltzer model, the anti-resonant reflecting optical waveguide (ARROW) model and the coupled-mode model are most commonly used to explain the guidance mechanism of NC-HCFs and other leaky HCFs.

A. Marcatili and Schmeltzer's Model

In 1964, Marcatili and Schmeltzer firstly analytically studied the mode properties of the dielectric HCF [22]. In their pioneering work, they derived formulas of mode attenuation and bending loss, which revealed the basic properties of modes in HCFs.

An idealized HCF consists of a circular core surrounding by infinite homogenous non-absorptive dielectric medium of higher refractive index than the core material (usually gas/vacuum). Due to the inverted refractive index contrast, total internal reflection cannot occur when the light is incident from the core at the interface between the core and cladding. The partial reflectivity at the core boundary indicates inevitable loss for light propagating in the core. The mode attenuation and corresponding propagation constant are written as [22],

$$\alpha_{\nu m} = \left(\frac{u_{\nu m}}{2\pi}\right)^2 \frac{\lambda^2}{r^3} \mathrm{Re}\left(V_\nu\right) \tag{1}$$

$$\beta_{\nu m} = \frac{2\pi}{\lambda}\left\{n_{\mathrm{core}} - \frac{1}{2}\left(\frac{u_{\nu m}\lambda}{2\pi r}\right)^2 \left[1 + \mathrm{Im}\left(\frac{V_\nu \lambda}{\pi r}\right)\right]\right\}. \tag{2}$$

Here $u_{\nu m}$ is the mth zero of the Bessel function $J_{\nu-1}$, and ν and m are azimuthal and radial number of modes; λ is the wavelength; r is the core radius; n_{core} is the refractive index of core medium; V_ν is the constant determined by the cladding refractive index and mode order [22].

Equations (1) and (2) are the most basic formulas to understand modes in all leaky HCFs. As r/λ grows bigger, the attenuation of modes is quickly reduced. For a mode of specific order, a higher propagation constant is required to satisfy the transverse resonance condition in a bigger core. Such larger core would give an increased glancing angle of light incident at the core boundary, which results in a higher Fresnel reflection. As a result, the mode in a larger core has a smaller attenuation.

Marcatili and Schmeltzer's model fails when complex structures are introduced to the cladding of HCF. The multiple reflections from the structured cladding can reduce or increase the attenuation of leaky modes by constructive/destructive interference, and it affects the dispersion of modes too.

B. ARROW Model

The ARROW model was firstly proposed in 1986 to explain the enhanced confinement in a planar waveguide with a series of high-low index regions forming the cladding [37]. In 2002 it was used to explain the light transmission in HC-PBG [38]. Soon it was being applied to a range of micro-structured HCFs.

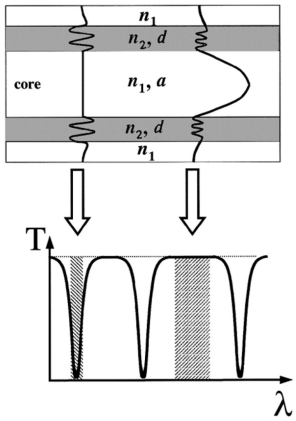

Fig. 2. Schematic of ARROW model. Top: structure of waveguide; Bottom: corresponding transmission spectrum [38].

The ARROW is 2-D model which can be extend to three dimensions. It approximates the cladding of HC-PBG as an array of high and low refractive index layers. Each higher refractive index layer can be considered as a Fabry–Perot resonator as in Fig. 2, which can enhance/decrease the confinement of light in the air core under different resonant/antiresonant conditions.

Assuming r/λ we have $\beta \approx 2\pi n_1/\lambda$ according to (2). In Fig. 2, the resonance wavelength is calculated as,

$$\lambda_m = \frac{2n_1 d}{m}\sqrt{\left(\frac{n_2}{n_1}\right)^2 - 1} \tag{3}$$

where n_1 and n_2 are low and high material refractive indices, respectively; d is the thickness of high index layer; and m is an integer, representing the order of resonance.

At the resonance wavelengths, the core mode experiences enhanced attenuation leaking through the high index layer. At wavelengths away from the resonance, the reflectivity of high index layer increases and the attenuation of the leaky mode is reduced. Therefore, the spectral transmission of ARROW waveguide features multiband transmission, similar to that of a Fabry–Perot resonator. The band edges of the transmission are well defined by the resonance wavelengths.

It is worth observing that the Bragg reflection cannot replace the ARROW model to explain HCFs [38]. Changing the pitch of the high index layers in the cladding barely shifts the band edge in simulations. This is also supported by the experimental demonstration of Kagome fiber. In Kagome fiber, it has been shown that reduction of the number of cladding layers does not significantly increase the fiber loss or shift the transmission band positions [36]. We conclude that the single-layer property of cladding plays a most important role when applying ARROW model to HCFs.

The loss edge of transmission bands can be precisely predicted by ARROW when $d/\lambda \gg 1$. At longer wavelengths, corresponding to the spectral range below the $m = 1$ resonance, the ARROW model is no longer useful.

The ARROW model is a well-established model which fits well with experimental results. Although it can precisely predict the band edge of transmission, it cannot provide further insight into the band properties.

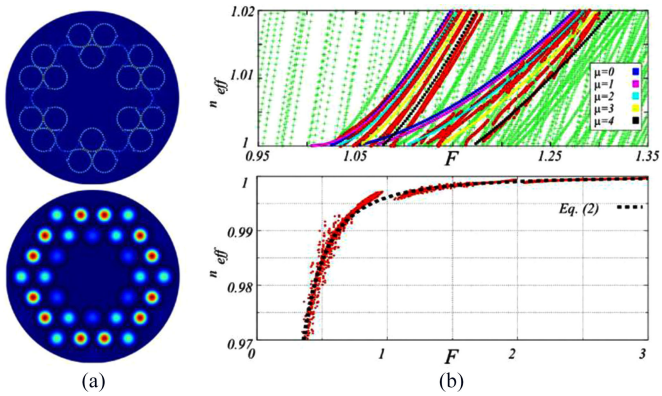

Fig. 3. Cladding mode characteristics in NC-HCF. (a) Intensity distribution of two types of cladding modes: a dielectric cladding mode (top) and a HE_{11}-like leaky air mode (bottom). (b) Effective indices of dielectric cladding modes (top) versus HE11-like leaky air mode. The black dotted line in (b) bottom is computed by Marcatili and Schmeltzer's model. Here *F* is normalized frequency by capillary thickness [41].

C. Coupled-Mode Model

The coupled-mode model applies coupled mode theory [39] to analyze the properties of HCFs based on Marcatili and Schmeltzer's model.

In real HCFs, the cladding is no longer an infinite and homogenous medium but has a complex configuration of refractive index distribution. The cladding modes are a set of modes including both dielectric modes (see Fig. 3(a) top) localized in the higher index regions and leaky air modes (see Fig. 3(a) bottom) inside lower index regions [40], [41]. In the coupled-mode model, the properties of core mode are interpreted as results of the longitudinal coupling with those cladding modes.

This method was successfully applied in analyzing the formation of bandgaps in HC-PBG [42]. By this method, inhibited coupling was proposed to explain the guidance in Kagome fiber [29]. In 2007, Argyros and his colleagues applied the coupled mode theory to the square lattice polymer HCF and quantitatively analyzed the formation of band edges of leaky HCF [43]. They pointed out that the absolute phase matching is not necessary to achieve an effective coupling between the cladding and core modes. $\Delta\beta \sim 10^{-4}$ m was found to be the threshold to estimate the transmission band edge, which matched well with the experimental measurement [43].

In 2012 Vincetti and Setti applied this method to NC-HCF and presented details of cladding mode features in NC-HCF [41]. Later, they used this method to demonstrate that the geometry of cladding elements was important to determine the confinement loss of HCFs. The polygonal shaped tube in the cladding adds extra loss due to the Fano-like coupling between the core and cladding modes [44]. This can be used to explain the different spectral features between NC-HCFs and Kagome fibers.

D. Function of Core Wall Shape

NC-HCFs are characterized by the negative curvature of the core wall, which has been numerically and experimentally demonstrated to effectively reduce the attenuation. Numerical simulations (Fig. 6) showed that in NC-HCF an increase of negative curvature influences the mode attenuation and even bending

loss in a complex way [45]. It has been confirmed that a large curvature of the core wall (small radius of curvature) can help decrease the overlap of core mode field with fiber materials to 10^{-4}. This has been experimentally and numerically demonstrated in silica NC-HCFs [9], [45] (further discussions will be found in Section IV-B).

Despite recent efforts in analytical analysis [46], the function of the core wall shape is not yet clear. It appears that both the properties of the high-index and of the low-index cladding modes are affected by the curvature.

IV. Guidance Properties—Mode Attenuation

A typical NC-HCF possesses multiple transmission bands, and the band edges are determined by the resonance wavelengths of cladding as described by the ARROW model. To experimentally study the fiber attenuation, we use the standard cutback method [47].

In HCFs there is no cutoff condition for high order modes. All modes exist at the same time but with different attenuations. High order modes are seldom observed in the propagation over long lengths because of their far higher attenuation and more sensitivity to the bending.

In the low order band of HC-NCF (determined by low order resonance wavelengths of cladding), because of relatively small r/λ ratio, the output is usually composed of the fundamental mode, or at most a few modes. By controlling the cutback length and the residual fiber length, the cutback method can be used to obtain a reliable measurement of fundamental mode attenuation.

In 2013, Yu and Knight reported a systematic study of the mode attenuation in one transmission band between the first and second resonant wavelengths in NC-HCFs with ice-cream-cone shape cladding [9]. 50 similar NC-HCFs drawn for different spectral ranges were fabricated and measured. Among them, the NC-HCFs with the minimum attenuation in their spectral ranges were selected for study [9]. Fig. 4 summarizes those minimum attenuations reported in [9] and latest results of this type of NC-HCFs [13], [18]. Table I lists detailed information of NC-HCFs in Fig. 4, including the figures of minimum attenuation and wavelengths, the spans of first transmission bands, and core diameters. The minimum attenuation 53.8 dB/km at 687.4 nm and the majority of core diameters are reported here for the first time.

In Fig. 4, the attenuation is dominated by different factors in different spectral ranges. Those factors include the material absorption at the longest wavelengths, leakage loss at mid-range wavelengths and "imperfection" loss at visible wavelengths and into the ultraviolet.

A. Leakage Loss

The leakage loss is the fundamental part of mode attenuation of NC-HCFs. Compared to conventional fibers, NC-HCF's are profoundly different in this respect because they have no strictly confined modes. By increasing r/λ, the mode attenuation can be effectively reduced according to (2). Generally, a NC-HCF with a large core can be expected to have lower loss.

According to (1), the leakage loss $\alpha \propto r^{-1}$ if r/λ remains constant. This is a natural result from the dimensional scaling law of electromagnetic field in HCFs [41]. All the fibers in Fig. 4 were designed and intended to be fabricated similarly, and expected to present similar structures but scaled for the different wavelengths of operation. In Table I, r/λ_m varies from 12.7 to 16.0 and the average is 14.6. Those fibers present high similarity apart from minor exceptions. We should therefor expect the minimum attenuation with wavelength to satisfy $\alpha \propto r^{-1}$. In Fig. 4, a fit to the data finds scaling with wavelengths as $\lambda^{-0.998}$ in the near-infrared spectrum from 1.2 to 3 μm, consistent with the assumption. At shorter and longer wavelengths, different dependences imply that different loss mechanisms other than leakage loss start to dominate, which will be discuss in Sections IV-B and IV-C.

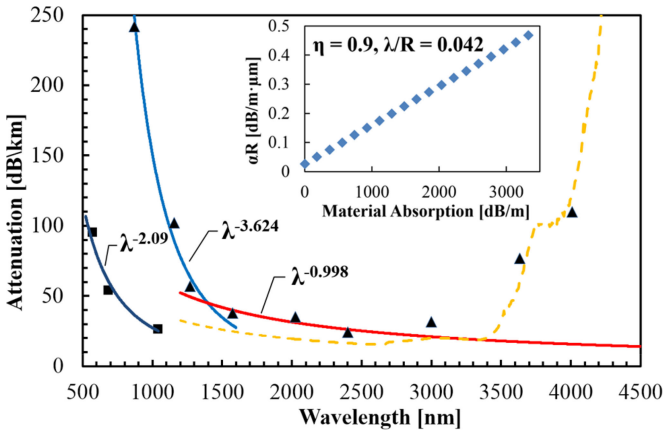

Fig. 4. Scaling of minimum attenuations with wavelengths of NC-HCFs. Measured data in [9] is shown as black triangles. Updated data is shown as black square [13], [18]. The dark blue, light blue and red solid lines represent fittings to selected points of attenuation $= A{\cdot}\lambda x$ with a resulting x of -2.09, -3.642 and -0.998 separately (dark blue curve fitting data points between 500 and 1040 nm; blue curve fitting data points between 700 and 1300 nm; red curve fitting points between 1500 to 2500 nm). The orange dashed line is total attenuation based on predictions of confinement losses from *Comsol* and scaled absorptive loss (measured). Inset: Simulation showing simulated variation in fiber attenuation as silica material absorption increases.

TABLE I
Data of NC-HCFs in Fig. 4

No.	Transmission Window [nm]	Minimum Attenuation Wavelength [nm]	Minimum Attenuation [dB/km]	Core Diameter [μm]	$\frac{r^*}{\lambda_m}$	References
1	470–610	571.2	95	16	14.0	[13]
2	600–850	687.4	53.8	22	16.0	new
3	870–1120	1041	26	32	15.4	[26]
4	750–890	869.35	242	22.5	12.9	[9]
5	970–1320	1158	102	38.3	16.5	[9]
6	1160–1520	1270	57	35	13.8	[9]
7	1500–1730	1576	38	46	14.6	[9]
8	1860–2530	2026	35	61	15.0	[9]
9	2200–2890	2400	24.4	61	12.7	[9]
10	2850–3850	3000	31.8	93	15.5	[3]
11	3400–4200	3635	76.7	108	14.8	[9]
12	3600–4400**	4010	110	119	14.8	[9]

Measured transmission windows of first band, minimum attenuations with wavelengths and core diameters of NC-HCFs in Fig. 4 are listed.

*r/λ_m is ratio of core radius over minimum attenuation wavelength.

**Measurement of transmission window was limited by light source intensity and detector response of monochromator.

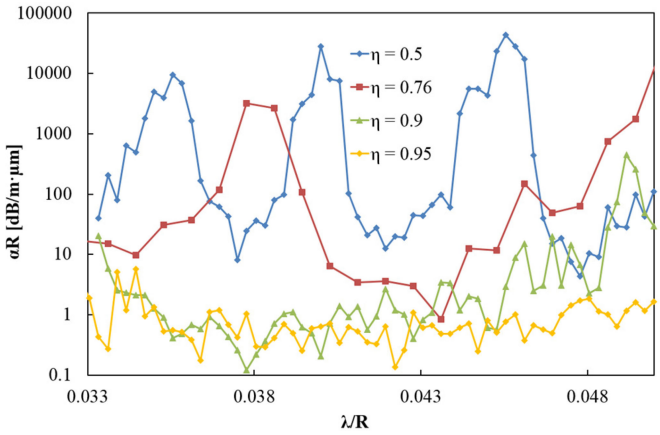

Fig. 5. Simulated normalized attenuation spectra of NC-HCF in different condition of η. η is defined as inner over outer diameter of capillary in the cladding. The bigger η is, the thinner core wall thickness is. Neither material absorption nor material dispersion is considered in those simulations. R is the core radius [9].

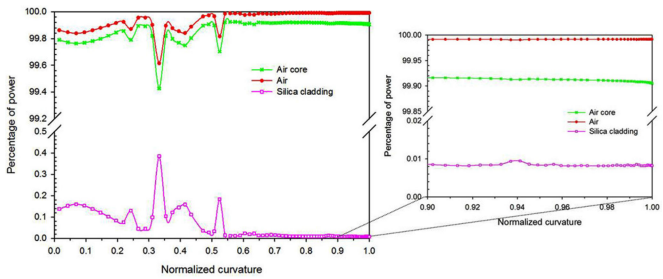

Fig. 6. Percentage of optical power in the air core (green line with "x"), in all the air holes of the fiber (red line with filled dots) and in the silica struts of the cladding (purple line with empty dots). On the right hand side is a magnification of the plot for curvature values between 0.9 and 1 [45].

In NC-HCF, reducing the core wall thickness is another important way to reduce the attenuation of NC-HCFs. Fig. 5 shows simulated attenuation spectra of NC-HCF for different core wall thicknesses [9]. Both axes are normalized by fiber core dimension. η is defined as the ratio of inner over outer diameter of capillary forming the core wall. The bigger η is, the thinner core wall thickness is. From Fig. 5, we observe that the leakage loss of NC-HCF is reduced with thinner core wall thickness. At the same time, the transmission window is wider, as predicted by ARROW model.

The leaky "airy" mode in the hollow regions of the cladding recently has been numerically demonstrated as another source of leakage loss [6], [32], [48]. The leakage loss in NC-HCFs can be further reduced and potentially reach 1 dB/km or even less by reducing the mode coupling between the core mode and air mode of cladding [6]. To reduce the coupling, extra capillary or finer structure can be added into cladding bores, shifting the air modes away from the propagation constant of the core and hence reducing the loss through this mechanism [6].

B. Material Absorption

In HCFs, because light is transmitted through the hollow core, the fiber material weakly influences the core mode properties, including the attenuation. The contribution of material absorption to the total loss in NC-HCFs arises from the mode overlap with the fiber material. Fig. 4 inset shows the simulated contribution to the mode attenuation in NC-HCF from the absorption of the cladding material. For a specific NC-HCF, the simulated mode attenuation increases linearly with material absorption, as expected for low absorption.

In NC-HCFs, it has been experimentally demonstrated that the mode overlap can be as low as 10^{-4} [9]. Numerical simulations agreed well with the experimental result (Fig. 6) [45]. Although the influence from fiber material in NC-HCF is tiny, material loss can still dominate the mode attenuation when material attenuation reaches thousands of dB/m.

Fused silica and softer glasses are the most common materials for fiber fabrication. Fused silica exhibits excellent transparency in the visible and near-infrared spectral regions, where the absorption of fiber material can be ignored [49]. However the phonon absorption increases quickly at longer wavelengths, and the material absorption rises rapidly from tens of dB/m at 3 μm to tens of thousands of dB/m beyond 5 μm wavelength [49], [50]. Such high loss is as the main factor limiting the performance of NC-HCFs at long wavelengths [3], [10], [11].

In Fig. 4, all NC-HCFs were made of F300 synthetic fused silica. 865 dB/m was measured at 4 μm wavelength [9]. The effect of material absorption on fiber loss is numerically estimated around 7000 times less than the material absorption due to the very low overlap of the guided mode with the glass at these long wavelengths by *Comsol*. By scaling the measured material absorption by this factor and adding it to the predicted leaky loss from *Comsol*, the total fiber loss was to increase rapid with material absorption and to dominate the attenuation of NC-HCF in this spectral range. Measured minimum attenuation was found to be 85 dB/km at 4 μm wavelength, which is measured as 10 000 times less than the measured silica absorption.

Soft-glasses, such as chalcogenides and fluorides, possess a much lower absorption in the mid-infrared region up to 10 μm and have been widely adopted as optical fiber materials for the mid-IR [23]. In 2000, the first use of soft-glass to fabricate HCF was demonstrated [51]. In 2010, more complex structured HC-PBG were successfully fabricated with chalcogenide glass [52].

Theoretically, because of the low material absorption, NC-HCFs made of soft-glasses should achieve much lower loss than those formed from silica at the long wavelengths in the mid-infrared. However, measured results were of the order of several dB/m or even worse [2]. Because of the very sensitive viscosity/temperature relation of soft-glass materials, it is technically challenging to obtain uniform and delicate holey structures in HCFs, which determines the optical properties of fibers. Compared with the mature state of silica fabrication, the processing routes for purification and fiber drawing still need improvement to achieve the theoretical performance limits for these materials.

C. "Imperfection" Loss

In the fabrication of HCFs, it has been the challenge to scale down the dimension for shorter wavelengths through the near-infrared and into the visible range. As the fiber gets smaller, the

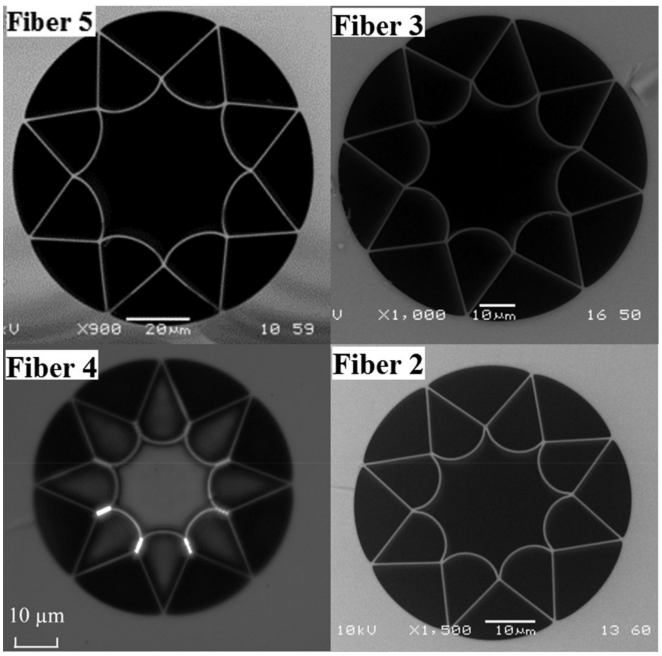

Fig. 7. SEM and optical microscope pictures of some NC-NCFs designed for similar transmission windows in Table I. SEM images of Fibers 5, 3 and 2, and an optical micrograph of Fiber 4 as labelled. Fibers 3 and 2 have lower attenuation than Fibers 4 and 5, respectively, despite being at approximately comparable wavelengths. The degradation of cladding structure, such as the slab-like fusion between capillaries (Fiber 4) and reduced boundary curvature (Fiber 5) may result in such higher losses. Fibers 3 and 2 were fabricated from the same preforms with fluorine-doped silica glass as the jacketing tube, and using a smaller draw-down ratio. Fibers 5 and 4 were fabricated using a pure silica glasses jacketing tube and a higher draw-down ratio.

balance between the surface tension and pressure in the fiber cladding becomes unstable, causing more frequent deformation leading to increased attenuation [53]. This extra loss of HCF arises from the "imperfection" of the fiber structure.

In Fig. 4, a substantial increase of attenuation is found in Fibers 4, 5, and 6 (see Table I) at shorter wavelengths [9]. They were drawn from a same group of preforms with dimension scaled for different transmission windows. To overcome the "imperfection" degradation, a smaller draw-down ratio was used to fabricate Fibers 1, 2 and 3 (see Table I). Also, in the fabrication of Fibers 1, 2 and 3, fluorine doped glass tubes rather than plain silica tubes were used to jacket the silica perform in the final draw to fiber. Comparing those drawn using a pure silica jacket, the fluorine-doped jacketed fibers exhibited much lower losses and less structural degradation, although they were no different from the silica fibers in dimensions. We attribute this to the reduced viscosity of the fluorine doped material, which enables the fiber to be drawn under more favorable conditions.

Fig. 7(a), (b) and (d) presents SEM images of Fiber 5, 3 and 2, and (c) is an optical microscope image of Fiber 4.

Fibers 5 and 3 (silica jacket) were both drawn for light transmission near 1 μm with similar core sizes. Fibers 4 and 2 (fluorine jacket) also have most parts of transmission bands overlapped between 750 and 850 nm. Fiber 3 exhibits a much lower attenuation than Fiber 5. The most significant difference can be found in core wall curvatures, which is also found in comparison between Fibers 4 and 2.

In Fiber 4, the fusion between capillaries has changed from points into slabs. Such defects are most common in small NC-HCFs for shorter wavelengths in the visible and near-infrared range. Extra "imperfection" loss was measured in Fiber 4 in comparison to Fiber 2. The degradation of fiber structure, including the slab fusion in cladding as well as flattened core wall curvatures, contributes to the increased attenuation at the short wavelengths.

In NC-HCF, there has been no experimental evidence relating the "imperfection" loss at short wavelengths to the scattering due to the surface roughness. But it may be worth in future to explore if such effect can be one factor limiting the attenuation performance of NC-HCFs at short wavelengths.

The scattering loss due to the core wall roughness has been identified as one of the reasons limiting the ultimate attenuation of HC-PBG [27], [54]. The surface roughness of core wall is inevitably formed along HCF because of the thermodynamics process in the fabrication, which is attributed to surface capillary wave frozen at the silica interface in the transition temperature range [55]. Such microscopic fluctuation is usually under one nanometer over a micrometric scale, but such roughness is enough to dominate the loss limit of HCFs, especially at short wavelengths.

The scattering effect causes the minimum attenuation with wavelengths to be proportional to λ^{-a} in log-log, where a may vary from 2.5 to 3.5 according to the design of the HC-PBG [27], [56].

V. Guidance Properties—Bending Loss

Generally, bending loss in optical fiber can be categorized into macro-bending and micro-bending according to the loss mechanism [47]. Micro-bending refers to the periodic or random deformations of the refractive-index distribution or of the geometry of optical fibers along the length, which can cause the energy to couple between the core modes and cladding modes if the deformations change sufficiently rapidly along the fiber axis [57]. The loss mechanism of micro-bending is essentially a scattering phenomenon, which is no interest of this section. The bending effect here refers to the macro-bending which accounts for the extra loss associated with the curved guidance when the fiber is bent.

The origin of bending loss of NC-HCF can be generally categorized as true bending loss, high order core mode conversion, and enhanced radiative/absorptive loss.

Kosolapov and colleagues numerically and experimentally demonstrated that at certain bending radii, the phase matching condition could be satisfied between the core and cladding air modes which resulted in extreme high losses [2]. Yu *et al.* found that the bending loss increased more rapidly at shorter wavelengths in the spectral transmission window [3]. This wavelength dependence was also experimentally observed in HC-PBG and all solid PBG [58], [59]. Setti *et al.* numerically found that the bending effect depended on wavelengths was due to the shift of band edge of transmission window to the longer

wavelengths [4]. Belardi *et al.* found that NC-HCF with open core boundary exhibited much less bending sensitivity than the other NC-HCFs [8]. Jaworski *et al.* measured the relation between the bending loss and the bending radius in NC-HCFs [13], [14]. In their study, low bend losses were found in NC-HCFs with lower mode attenuations [13].

A. True Bend Loss

In Marcatili and Schmeltzer's model, such loss can be determined by a perturbation correction of mode attenuation of a straight fiber in the bending condition [22]. The bending loss is written as,

$$\alpha_{\nu m} = \frac{r^3}{\lambda^2 R^2} \mathrm{Re} V_{\nu m}. \tag{4}$$

Here R is the bending radius.

Equation (4) clearly shows that the bending loss grows faster than the bending curvature. For a specific fiber, at one wavelength, $\alpha_{\nu m} \propto R^{-2}$ This bending loss dependence was also demonstrated by numerical simulations in NC-HCF [4] and matched with the observations in measurements [3], [8], [13], [14].

According to (4), the bend loss can be traded off with leakage loss as a function of core size. In the fiber design, to achieve lower transmission loss, a large core is preferable however it inevitably causes a higher bending loss.

B. High Order Core Mode Conversion

In 1969, Marcatili pointed out that higher order mode conversion is the main loss mechanism in the high refractive index core waveguide [60]. He demonstrated that, under multimode guidance, the loss originating from high order mode conversion is many orders of magnitude larger than the radiated loss of the fundamental mode because of bending [60].

NC-HCF exhibits lossy multimode guidance properties. The high order mode conversion is a significant reason for high bending loss in NC-HCFs. More work is needed to investigate such effects in HCFs.

C. Enhanced Radiative/Absorptive Loss

The coupling between the core and cladding modes can be greatly enhanced at specific wavelengths in the bent condition. On one hand, the phase matching condition can be satisfied or nearly satisfied between the core mode and cladding modes in the bent fiber. This has been observed both numerically and experimentally [2], [4], [61]. Such resonances cause well-defined and significant loss peaks in the transmitted spectrum.

On the other hand, bending also increases the overlap between core mode and cladding material. With the method of conformal transformation [62], the equivalent refractive index distribution of NC-HCF under bending makes core modes closer to one side of the core. At long wavelengths where the fiber material is absorptive or at short wavelengths where surface roughness of core wall causes dramatic scattering loss, there may be an associated increase in observed bend loss.

TABLE II
MEASURED BENDING LOSS OF NC-HCFS

No. in Fig. 4	Measured Wavelength [nm]	Bending Loss [dB/m]	Bending Radius [cm]	References
1*	515	190.0	0.5	[13]
		3.2	2.5	
	532	216.4	0.5	
		5.1	2.5	
2*	1064	35.6	2.5	[14]
		2.6	6	
3**	3100–3200	< 3.18	2.5	[8]
		0.3	7.96	

*The bending loss of NC-HCFs were measured by bending a piece of NC-HCF by 180° with two ends kept straight.

**The fiber was bent into a coil and bending loss was calculated by dividing the total bending-induced loss by the number of coils.

VI. GUIDANCE PROPERTIES—DISPERSION AND NONLINEARITY

In NC-HCF, the group velocity dispersion and nonlinearity are tiny, and the modal dispersion is relatively low. The material contribution to the overall dispersion and nonlinearity is very limited due to the reduced overlap between the core mode field and cladding region.

Although no direct measurements have been reported, the extremely low dispersion and nonlinearity of NC-HCFs have been demonstrated in experiments [13], [14], [18]. A 6 ps laser pulse at 1030 nm with nearly 92 μJ pulse energy was stretched to 8.7 ps after 8 m propagation in Fiber 5 in Table I [14]. Such pulse length stretching could be only caused by modal dispersion rather than group delay dispersion. No pulse stretching was found in delivering 6 ps laser pulse at 515 nm with 30 μJ pulse energy in Fiber 1 in Table II [13].

Because of their low dispersion and nonlinearity, NC-HCFs can provide appropriate solutions to high power/ultrafast laser delivery in fundamental scientific research and in industrial applications.

A. Dispersion

The modal group delay and group velocity dispersion can be calculated in Marcatili and Schmeltzer's model.

According to (2), the group velocity dispersion should stay anomalous and extremely low over the whole spectral range if we assume the core medium is non-dispersive. By adding different types of gases and changing the gas pressure, the total dispersion of core can be tuned over a certain range [63].

The flat and shallow dispersion slope changes rapidly at wavelengths near band edges where cladding modes couple with the core mode. As in HC-PBG, the strong coupling interaction at the band edges causes the group dispersion across the transmission window to change from anomalous to normal towards shorter wavelengths [64]. Near the band edge, the value of group velocity dispersion rises rapidly up to hundreds of $\mathrm{ps}/(\mathrm{km} \times \mathrm{nm})$. Based on anti-crossing coupling, a method of tailoring the dispersion of HC-PBG has been proposed by tuning the size of subsidiary bores around the core in the cladding [65], [66].

B. Nonlinearity

Nonlinearity of NC-HCFs comes from the gas inside the core and part of the cladding material. Air, for example, has Kerr nonlinearity in roughly three orders of magnitude less than in silica [67]. The cladding material contributes to nonlinearity due to the limited overlap between the core mode and cladding material. For NC-HCFs, the overlap between the core mode and cladding material approaches to 0.01%, in which we can expect the residual nonlinearity from the fiber material can be ignored. As a result, the main source of nonlinearity will only come from the air/gas filling the core, unless the gas pressure is low.

VII. Applications

NC-HCFs have been already successfully used in high power laser transmission at various wavelengths from the visible to mid-infrared. They have also been demonstrated as a competitive candidate to replace gas cell/tube in the study of gas-light interactions.

A. Laser Transmission

In the far-infrared spectrum, CO_2 laser transmission at 10.6 μm was demonstrated by the NC-HCF made of $As_{30}Se_{50}Te_{20}$ glass in 2011 [2]. A single-mode-like guidance was measured in less than 1 m fiber with about 11 dB/m attenuation at 10.6 μm. When the fiber was bent to a radius of 30 cm, the deformation of mode distribution was observed [2].

In the mid-infrared spectrum, the delivery of high energy pulses laser pulses at 2.94 μm, with energies up to 195 mJ (limited by laser power), at a pulse length of 225 μs was successfully demonstrated through a silica NC-HCF in 2013 [10]. At 2.94 μm, high power Er:YAG laser have been used in biological tissue ablation in medical surgery because of high absorption coefficient of water molecules. In practical applications, a flexible guide from the laser source to the patient will allow more freedom for surgeons. NC-HCF developed for the experiment exhibited low attenuation of 0.183 dB/m at 2.94 μm. Single mode guidance was measured at the output of fiber from 6.8 to 0.8 m fiber length. This fiber also presented typically low numerical aperture (NA) of 0.03 which was determined by the large core size (94 μm in diameter). The small divergence of laser beam would allow longer working distance which could add more freedom in the practical surgical application.

In the near-infrared, picosecond and nanosecond pulse delivery at 1030 and 1064 nm wavelengths were reported through a silica NC-HCF in 2013 [14]. Picosecond pulses with an average power above 36 W and energies of 92 μJ were delivered in NC-HCF. No optical damage to the NC-HCF was found during nanosecond pulse delivery and the fiber was expect to be capable of delivering at least 8 mJ in a 60 ns pulse before damage. 0.03 NA was also measured in the fiber.

In the visible, deliver of high energy nanosecond and picosecond pulses in the green spectral region was also demonstrated successfully in 2015, which aimed for precision micro-machining and marking of metals and glasses [13]. The fabricated NC-HCF had attenuations of 0.15 and 0.18 dB/m at 532 and 515 nm, respectively. It achieved transmission of 6 ps pulses at 515 nm with a maximum energy of 30 μJ and an average power of 12 W, which was more than double record reported in Kagome fiber at this wavelength at that time [68]. The NC-HCF also provided a stable single-mode output, with very low bend sensitivity. The measured results showed that no degradation of temporal and spectral properties of the guided beam were detected. 0.038 NA was measured in the fiber.

B. Gas Hollow Core Fiber Laser

Gas hollow core fiber laser is a novel fiber laser which makes use of an atomic/molecular gas as a gain medium confined in a length of NC-HCF [69].

The advantages of using HCF instead of a traditional gas cell in developing a gas laser is that the interaction length could be extended, low thresholds and high efficiencies can be expected, and fiber-based systems have great potential for integration and reduction in size.

Compared with conventional solid fiber lasers, gas HCF lasers will remove the nonlinear and damage limits which arise because of the interaction between the light and solid material. Thermal effects, such as thermal lensing under high power operation may be finally conquered in gas fiber lasers. A variety of atomic/molecular gases provides a broad spectral range of emission wavelengths, from the UV to the IR. Owing to the nature of atomic and molecular gas transitions, the gas HCF laser always presents a much narrower laser spectral bandwidth than the solid fiber lasers.

In 2013 a Raman NC-HCF laser was firstly reported [15]. The simulated Raman scattering (SRS) at 1.9 μm was generated in a 6.5 m long H_2-filled NC-HCF at 23 bars, pumped by a 1064 nm microchip laser. By proper design, a silica NC-HCF can guide both Stokes and pump light with low loss in two different transmission bands. 1500 W peak power of pure vibrational Stokes SRS at 1907 nm was measured with a corresponding quantum conversion efficiency above 48%.

In 2014, Wang *et al.* reported that 3.1–3.2 μm mid-infrared emission was achieved in the single pass of silica NC-HCF filled with acetylene gas pumped by an amplified, modulated, narrowband, tunable 1.5 μm diode laser [17]. The maximum power conversion efficiency of the single-pass amplified spontaneous emission (ASE) was approximate 30%, with respect to the absorbed pump power in a 10.5 m length of fiber at pressure of 0.7 mbar. The minimum pump laser energy required was less than 50 nJ. Based on Wang's experiment scheme, a 3.16 μm acetylene-filled silica NC-HCF laser was recently demonstrated [20]. 101 m silica NC-NCF of extremely low loss at the lasing wavelength (25 dB/km) was added as a feedback fiber to form a ring cavity with the acetylene filled gain fiber. By synchronous pump with narrow line 1.53 μm pulses, pulsed lasing at 3.16 μm was finally obtained. The high damage threshold and low nonlinearity of NC-HCF suggested good potential of power scaling.

Besides optically-pumped lasers, traditional electrical gas discharge for gas lasers are also being explored in gas NC-HCF

lasers. Optical gain has been measured in NC-HCFs filled with Helium–Xenon gases by dc electrical discharge [16], [19].

VIII. Remarks

This paper describes the very rapid progress made over the last few years in developing new forms of hollow optical fiber, and gives early indication of their potential applications. It is not comprehensive, and we hope and expect that it will become rapidly out of date with the continuing progress in fiber design, fabrication and application. The work so far opens up a range of possible future directions, and we expect further rapid progress will lead to yet more potential applications. Nonetheless, progress so far has already shown that it is possible to design simple novel fibers which can outperform conventional optical fibers in many ways.

Acknowledgment

The authors would like to thank C. Harvey for providing the SEM picture in Fig. 7(b).

References

[1] A. D. Pryamikov *et al.*, "Demonstration of a waveguide regime for a silica hollow–core microstructured optical fiber with a negative curvature of the core boundary in the spectral region >3.5 μm," *Opt. Exp.*, vol. 19, no. 2, pp. 1441–1448, Jan. 2011.

[2] A. F. Kosolapov *et al.*, "Demonstration of CO_2-laser power delivery through chalcogenide-glass fiber with negative-curvature hollow core," *Opt. Exp.*, vol. 19, no. 25, pp. 25723–25728, Dec. 2011.

[3] F. Yu, W. J. Wadsworth, and J. C. Knight, "Low loss silica hollow core fibers for 3–4 μm spectral region," *Opt. Exp.*, vol. 20, no. 10, pp. 11153–11158, May 2012.

[4] V. Setti, L. Vincetti, and A. Argyros, "Flexible tube lattice fibers for terahertz applications," *Opt. Exp.*, vol. 21, no. 3, pp. 3388–3399, Feb. 2013.

[5] A. N. Kolyadin *et al.*, "Light transmission in negative curvature hollow core fiber in extremely high material loss region," *Opt. Exp.*, vol. 21, no. 8, pp. 9514–9519, Apr. 2013.

[6] W. Belardi and J. C. Knight, "Hollow antiresonant fibers with reduced attenuation," *Opt. Lett.*, vol. 39, no. 7, pp. 1853–1856, Apr. 2014.

[7] V. S. Shiryaev, "Chalcogenide glass hollow-core microstructured optical fibers," *Frontiers Mater.*, vol. 2, art. no. 24, Mar. 2015.

[8] W. Belardi and J. C. Knight, "Hollow antiresonant fibers with low bending loss," *Opt. Exp.*, vol. 22, no. 8, pp. 10091–10096, Apr. 2014.

[9] F. Yu and J. C. Knight, "Spectral attenuation limits of silica hollow core negative curvature fiber," *Opt. Exp.*, vol. 21, no. 18, pp. 21466–21471, Sep. 2013.

[10] A. Urich *et al.*, "Flexible delivery of Er: YAG radiation at 2.94 μm with negative curvature silica glass fibers: A new solution for minimally invasive surgical procedures," *Biomed., Opt. Exp.*, vol. 4, no. 2, pp. 193–205, Feb. 2013.

[11] A. Urich *et al.*, "Silica hollow core microstructured fibres for mid-infrared surgical applications," *J. Non-Cryst. Solids*, vol. 377, pp. 236–239, Oct. 2013.

[12] J. D. Shephard *et al.*, "Silica hollow core microstructured fibers for beam delivery in industrial and medical applications," *Frontiers Phys.*, vol. 3, art. no. 10, Apr. 2015.

[13] P. Jaworski *et al.*, "High energy green nanosecond and picosecond pulse delivery through a negative curvature fiber for precision micromachining," *Opt. Exp.*, vol. 23, no. 7, pp. 8498–8506, Mar. 2015.

[14] P. Jaworski *et al.*, "Picosecond and nanosecond pulse delivery through a hollow-core negative curvature fiber for micro-machining applications," *Opt. Exp.*, vol. 21, no. 19, pp. 22742–22753, Sep. 2013.

[15] Z. Wang, F. Yu, W. J. Wadsworth, and J. C. Knight, "Efficient 1.9 μm emission in H_2-filled hollow core fiber by pure stimulated vibrational Raman scattering," *Laser Phys. Lett.*, vol. 11, no. 10, p. 105807, Oct. 2014.

[16] S. A. Bateman, W. Belardi, F. Yu, C. E. Webb, and W. J. Wadsworth, "Gain from Helium-Xenon discharges in hollow optical fibres at 3.5 μm," presented at the Advanced Photonics Conf., Barcelona, Spain, 2014, Paper SoM4B.3.

[17] Z. Wang, W. Belardi, F. Yu, W. J. Wadsworth, and J. C. Knight, "Efficient diode-pumped mid-infrared emission from acetylene-filled hollow-core fiber," *Opt. Exp.*, vol. 22, no. 18, pp. 21872–21878, Sep. 2014.

[18] C. Harvey, F. Yu, J. C. Knight, W. Wadsworth, and P. Almeida, "Reducing nonlinear limitations of ytterbium mode-locked fibre lasers with hollow-core negative curvature fibre," presented at the Conf. Lasers Electro-Optics, San Jose, CA, USA, 2015, Paper STh1L.5.

[19] A. Love, S. Bateman, W. Belardi, C. Webb, and W. Wadsworth, "Double pass gain in helium-xenon discharges in hollow optical fibres at 3.5 μm," presented at the Conf. Lasers Electro-Optics, San Jose, CA, USA, 2015, Paper SF2F.4.

[20] M. R. Abu Hassan *et al.*, "Synchronously pumped mid-IR hollow core fiber gas laser," presented at the Conf. Lasers Electro-Optics, San Jose, CA, USA, 2015, Paper SF1F.7.

[21] J. R. Carson, S. P. Mead, and S. A. Schelkunoof, "Hyper-frequency wave guides-mathematical theory," *J. Bell Syst. Technol.*, vol. 15, pp. 310–333, 1936.

[22] E. Marcatili and R. Schmeltzer, "Hollow metallic and dielectric waveguides for long distance optical transmission and lasers," *Bell Syst. Tech. J.*, vol. 43, no. 4, pp. 1783–1809, 1964.

[23] J. A. Harrington, "A review of IR transmitting, hollow waveguides," *Fiber Integr. Opt.*, vol. 19, no. 3, pp. 211–227, Jul. 2000.

[24] J. C. Knight, "Photonic band gap guidance in optical fibers," *Science*, vol. 282, no. 5393, pp. 1476–1478, Nov. 1998.

[25] P. S. J. Russell, "Photonic-crystal fibers," *J. Lightw. Technol.*, vol. 24, no. 12, pp. 4729–4749, Dec. 2006.

[26] B. J. Mangan *et al.*, "Low loss (1.7 dB/km) hollow core photonic bandgap fiber," presented at the *Optical Fiber Communication Conf.*, Los Angeles, CA, USA, 2004, vol. 2.

[27] P. J. Roberts *et al.*, "Ultimate low loss of hollow-core photonic crystal fibres," *Opt. Exp.*, vol. 13, no. 1, pp. 236–244, Jan. 2005.

[28] F. Benabid, J. C. Knight, G. Antonopoulos, and P. S. J. Russell, "Stimulated Raman scattering in hydrogen-filled hollow-core photonic crystal fiber," *Science*, vol. 298, no. 5592, pp. 399–402, 2002.

[29] F. Benabid and P. J. Roberts, "Linear and nonlinear optical properties of hollow core photonic crystal fiber," *J. Mod. Opt.*, vol. 58, pp. 37–41, 2011.

[30] Y. Y. Wang, F. Couny, P. J. Roberts, and F. Benabid, "Low loss broadband transmission in optimized core-shape Kagome hollow-core PCF," in *Proc. Lasers Electro-Opt., Quantum Electron. Laser Sci. Conf.*, 2010, pp. 1–2.

[31] Y. Y. Wang, N. V Wheeler, F. Couny, P. J. Roberts, and F. Benabid, "Low loss broadband transmission in hypocycloid-core Kagome hollow-core photonic crystal fiber," *Opt. Lett.*, vol. 36, no. 5, pp. 669–671, Mar. 2011.

[32] J. C. Knight, W. Belardi, and F. Yu, "Out of the blue and into the black—Silica fibres for the mid-IR," presented at the Advanced Solid State Lasers Conf., Shanghai, China, 2014, Paper AW3A.4.

[33] W. Belardi, "Design and properties of hollow antiresonant fibers for the visible and near infrared spectral range," *J. Lightw. Technol.*, vol. 32, no. 21, pp. 4497–4503, Nov. 2015.

[34] B. Debord *et al.*, "Hypocycloid-shaped hollow-core photonic crystal fiber Part I: Arc curvature effect on confinement loss," *Opt. Exp.*, vol. 21, no. 23, pp. 28597–28608, Nov. 2013.

[35] M. Alharbi *et al.*, "Hypocycloid-shaped hollow-core photonic crystal fiber Part II: Cladding effect on confinement and bend loss," *Opt. Exp.*, vol. 21, no. 23, pp. 28609–28616, 2013.

[36] F. Gérôme, R. Jamier, J.-L. Auguste, G. Humbert, and J.-M. Blondy, "Simplified hollow-core photonic crystal fiber," *Opt. Lett.*, vol. 35, no. 8, pp. 1157–1159, Apr. 2010.

[37] M. A. Duguay, Y. Kokubun, T. L. Koch, and L. Pfeiffer, "Antiresonant reflecting optical waveguides in SiO2-Si multilayer structures," *Appl. Phys. Lett.*, vol. 49, no. 1, p. 13, Jul. 1986.

[38] N. M. Litchinitser, A. K. Abeeluck, C. Headley, and B. J. Eggleton, "Antiresonant reflecting photonic crystal optical waveguides," *Opt. Lett.*, vol. 27, no. 18, pp. 1592–1594, Sep. 2002.

[39] A. W. Snyder and J. D. Love, *Optical Waveguide Theory*. London, U.K.: Chapman & Hall, 1983.

[40] F. Couny, F. Benabid, P. J. Roberts, M. T. Burnett, and S. A. Maier, "Identification of Bloch-modes in hollow-core photonic crystal fiber cladding," *Opt. Exp.*, vol. 15, no. 2, pp. 325–338, Jan. 2007.

[41] L. Vincetti and V. Setti, "Waveguiding mechanism in tube lattice fibers," *Opt. Exp.*, vol. 18, no. 22, pp. 23133–23146, Oct. 2010.

[42] T. A. Birks, G. J. Pearce, and D. M. Bird, "Approximate band structure calculation for photonic bandgap fibres," *Opt. Exp.*, vol. 14, no. 20, pp. 9483–9490, Oct. 2006.
[43] A. Argyros and J. Pla, "Hollow-core polymer fibres with a kagome lattice: Potential for transmission in the infrared," *Opt. Exp.*, vol. 15, no. 12, p. 7713–7719, Jun. 2007.
[44] L. Vincetti and V. Setti, "Extra loss due to Fano resonances in inhibited coupling fibers based on a lattice of tubes," *Opt. Exp.*, vol. 20, no. 13, pp. 14350–14361, Jun. 2012.
[45] W. Belardi and J. C. Knight, "Effect of core boundary curvature on the confinement losses of hollow antiresonant fibers," *Opt. Exp.*, vol. 21, no. 19, pp. 21912–21917, Sep. 2013.
[46] A. D. Pryamikov, "Negative curvature hollow core fibers: Design, fabrication, and applications," in *Proc. SPIE*, 2014, vol. 8961, pp. 1–11.
[47] J. A. Buck, *Fundamentals of Optical Fibers*, 2nd ed. Hoboken, NJ, USA: Wiley, 2004.
[48] F. Poletti, "Nested antiresonant nodeless hollow core fiber," *Opt. Exp.*, vol. 22, no. 20, pp. 23807–23828, Oct. 2014.
[49] R. Kitamura, L. Pilon, and M. Jonasz, "Optical constants of silica glass from extreme ultraviolet to far infrared at near room temperature," *Appl. Opt.*, vol. 46, no. 33, pp. 8118–8133, Nov. 2007.
[50] O. Humbach, H. Fabian, U. Grzesik, U. Haken, and W. Heitmann, "Analysis of OH absorption bands in synthetic silica," *J. Non-Cryst. Solids*, vol. 203, pp. 19–26, Aug. 1996.
[51] T. M. Monro, Y. D. West, D. W. Hewak, N. G. R. Broderick, and D. J. Richardson, "Chalcogenide holey fibres," *Electron. Lett.*, vol. 36, no. 24, pp. 1998–2000, 2000.
[52] F. Désévédavy *et al.*, "Chalcogenide glass hollow core photonic crystal fibers," *Opt. Mater.*, vol. 32, no. 11, pp. 1532–1539, Sep. 2010.
[53] P. J. Mosley *et al.*, "Ultrashort pulse compression and delivery in a hollow-core photonic crystal fiber at 540 nm wavelength," *Opt. Lett.*, vol. 35, no. 21, pp. 3589–3591, 2010.
[54] F. Poletti *et al.*, "Towards high-capacity fibre-optic communications at the speed of light in vacuum," *Nature Photon.*, vol. 7, pp. 279–284, 2013.
[55] T. Sarlat, A. Lelarge, E. Søndergård, and D. Vandembroucq, "Frozen capillary waves on glass surfaces: An AFM study," *Eur. Phys. J. B*, vol. 54, no. 1, pp. 121–126, 2006.
[56] E. Fokoua *et al.*, "Analysis of light scattering from surface roughness in hollow-core photonic bandgap fibers," *Opt. Exp.*, vol. 20, no. 19, pp. 20980–20991, Jan. 2012.
[57] D. Marcuse, "Microdeformation losses of single-mode fibers," *Appl. Opt.*, vol. 23, no. 7, pp. 1082–1091, Apr. 1984.
[58] T. P. Hansen *et al.*, "Air-guiding photonic bandgap fibers: Spectral properties, macrobending loss, and practical handling," *J. Lightw. Technol.*, vol. 22, no. 1, pp. 11–15, 2004.
[59] T. A. Birks *et al.*, "Bend loss in all-solid bandgap fibres," *Opt. Exp.*, vol. 14, no. 12, pp. 5688–5698, 2006.
[60] E. A. J. Marcatili, "Bends in optical dielectric guides," *Bell Syst. Tech. J.*, vol. 48, no. 7, pp. 2103–2132, Sep. 1969.
[61] G. K. Alagashev *et al.*, "Impact of geometrical parameters on the optical properties of negative curvature hollow-core fibers," *Laser Phys.*, vol. 25, no. 5, p. 055101, May 2015.
[62] M. Heiblum and J. Harris, "Analysis of curved optical waveguides by conformal transformation," *IEEE J. Quantum Electron.*, vol. 11, no. 2, pp. 75–83, Feb. 1975.
[63] P. S. J. Russell, P. Hölzer, W. Chang, A. Abdolvand, and J. C. Travers, "Hollow-core photonic crystal fibres for gas-based nonlinear optics," *Nature Photon.*, vol. 8, no. 4, pp. 278–286, Mar. 2014.
[64] M. G. Welch, C. E. de Nobriga, R. A. Correa, W. J. Wadsworth, and J. C. Knight, "Accurate measurement of the dispersion of hollow-core fibers using a scalable technique," *Opt. Exp.*, vol. 17, no. 11, pp. 9006–9012, May 2009.
[65] P. J. Roberts, "Control of dispersion in hollow core photonic crystal fibers," presented at the Conf. Lasers Electro-Optics, Baltimore, MD, USA, 2007, Paper CWF2.
[66] J. Lægsgaard, P. J. Roberts, and M. Bache, "Tailoring the dispersion properties of photonic crystal fibers," *Opt. Quantum Electron.*, vol. 39, no. 12/13, pp. 995–1008, 2007.
[67] D. G. Ouzounov *et al.*, "Generation of megawatt optical solitons in hollow-core photonic band-gap fibers," *Science*, vol. 301, no. 5640, pp. 1702–1704, Sep. 2003.
[68] B. Debord *et al.*, "Ultra low-loss hypocycloid-core Kagome hollow-core photonic crystal fiber for green spectral-range applications," *Opt. Lett.*, vol. 39, no. 21, pp. 6245–6248, Nov. 2014.
[69] A. V. V. Nampoothiri *et al.*, "Hollow-core optical fiber gas lasers (HOFGLAS): A review," *Opt. Mater. Exp.*, vol. 2, no. 7, pp. 948–961, Jun. 2012.

Fei Yu was born in China, in 1986. He received the B.S. and M.S. degrees in physics electronics from the Beijing Institute of Technology, Beijing, China, in 2008 and 2010, respectively, and the Ph.D. degree in optics from the University of Bath, Bath, U.K., in 2014.

Since 2014, he has been working as a Research Officer with the University of Bath. His research interests include optical fiber design and applications

Jonathan C. Knight received the Ph.D. degree in Cape Town. He was a Postdoctoral Researcher with the Ecole Normale Superieure, Paris, France, and the University of Southampton. He is currently a Professor at the Department of Physics, University of Bath, Bath, U.K., where he is involved in new forms of optical fibers and their applications.